

Epipolar-Guided Deep Object Matching for Scene Change Detection

Kento Doi^{*†}, Ryuhei Hamaguchi[†], Shun Iwase[†], Rio Yokota[†], Yutaka Matsuo^{*}, Ken Sakurada[†]

^{*} The University of Tokyo, Tokyo, Japan

[†] National Institute of Advanced Industrial Science and Technology (AIST), Tokyo, Japan

Abstract—This paper describes a viewpoint-robust object-based change detection network (OBJ-CDNet). Mobile cameras such as drive recorders capture images from different viewpoints each time due to differences in camera trajectory and shutter timing. However, previous methods for pixel-wise change detection are vulnerable to the viewpoint differences because they assume aligned image pairs as inputs. To cope with the difficulty, we introduce a deep graph matching network that establishes object correspondence between an image pair. The introduction enables us to detect object-wise scene changes without precise image alignment. For more accurate object matching, we propose an epipolar-guided deep graph matching network (EGMNet), which incorporates the epipolar constraint into the deep graph matching layer used in OBJ-CDNet. To evaluate our network’s robustness against viewpoint differences, we created synthetic and real datasets for scene change detection from an image pair. The experimental results verified the effectiveness of our network.

I. INTRODUCTION

Scene change detection has been exhaustively studied in the fields of computer vision and remote sensing for practical applications, such as anomaly detection, infrastructure inspection, and disaster prevention using images from satellites or surveillance cameras. In recent years, the need for such research is increasing rapidly because maps must be kept up to date in applications of self-driving cars, augmented reality, and service robots. Specifically, for the navigation of autonomous vehicles, precise assessment of the latest landmarks is crucial, however, it is infeasible to manually update the maps for large city areas. As an alternative, the previous studies [1]–[8] have presented methods using images taken by vehicle-mounted cameras to automatically detect the change regions.

Most of the methods require precise alignment to detect pixel-wise changes between input images taken at different times and cameras. In cases of satellite and surveillance cameras, viewpoint differences among images are generally small and easy to calibrate. On the other hand, in cases of images captured by vehicle-mounted cameras, precise alignment is difficult since camera trajectory and shutter timing cannot be replicated across time. Moreover, pixel-wise methods are vulnerable to illumination changes.

One possible solution to the difficulty of aligning images captured by vehicle-mounted cameras is to perform depth estimation. However, it is theoretically impossible to reconstruct the depth of the scene by stereo matching from an image pair with scene changes. Another possible strategy is the monocular depth estimation, but it is difficult

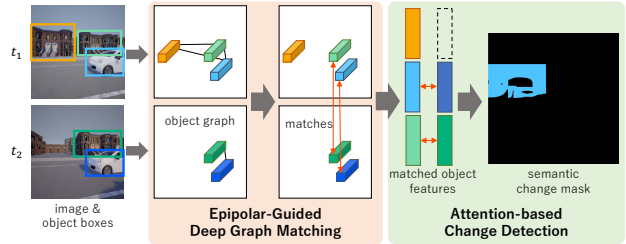


Fig. 1. The overview of our object-based change detection network (OBJ-CDNet). Given an image pair and object detection boxes, we first establish object correspondences between images with deep graph matching which incorporates the epipolar constraint. Then, the attention-based network estimates the semantic change mask from matched object features. The OBJ-CDNet can learn the pixel-wise semantic change detection but requires only bounding boxes and correspondences of them as supervision.

to accurately estimate the depth of thin objects such as streetlights and advertisement.

To alleviate the difficulty, we propose an object-based change detection network (OBJ-CDNet) with deep graph matching (Fig. 2). Instead of precisely aligning input images, the OBJ-CDNet first extract object graphs from each image and applies deep graph matching to the graphs to detect object-wise scene changes. The method effectively incorporate epipolar constraint into the deep graph matching, which further improves robustness to viewpoint differences. By introducing an attention mechanism into the change detection network, the OBJ-CDNet can estimate pixel-wise changes without need for pixel-wise change annotations. Furthermore, the OBJ-CDNet can be extended to estimate finer pixel-wise changes by replacing the attention module with a semantic segmentation network [9] pre-trained with a semantic segmentation dataset, such as Cityscapes dataset [10]. This extension can significantly reduce the amount of work required to create the dataset because labeling object-wise changes is much easier than pixel-wise ones while it achieves accuracy similar to fully-supervised methods that require pixel-wise change annotations.

Additionally, to evaluate our method, we created both synthetic and real datasets for object change detection, called CARLA- and GSV-OBJCD ¹. They consist of 15,000 and 500 scene perspective image pairs of CARLA [11] and Google Street View images, respectively, with object bounding boxes and matching, the presence of change, pixel-level change map and object category annotation. To the best of

¹CARLA-OBJCD dataset and the annotations of GSV-OBJCD dataset will be publicly available.

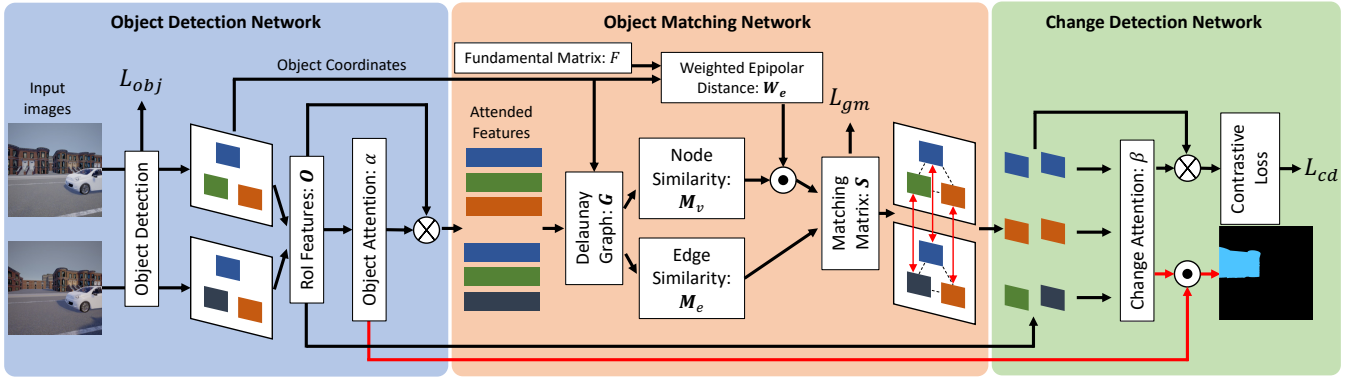


Fig. 2. The details of our object-based change detection network (OBJ-CDNet). OBJ-CDNet is made up of three major components: the *object detection network* (Section III-B), the *object matching network* (Sections III-C and III-D), and the *change detection network* (Section III-E). The first component takes an image pair as input and predicts bounding boxes of objects in the scene. Then, object graphs are created from detected bounding boxes and image feature maps. The object matching layer creates an affinity matrix from the object graphs and a fundamental matrix and finds the optimal correspondences between objects. The final component uses an attention-based network to estimate a semantic change mask from the matched object features.

our knowledge, CARLA-OBJCD dataset is the first publicly available large scale synthetic dataset for street-level scene change detection.

Our main contributions are as follows:

- We propose an object-based change detection network utilizing deep graph matching that can also estimate pixel-wise changes with only object-wise change annotation.
- We propose the epipolar-guided deep graph matching network (EGMNet), in which the epipolar constraint is incorporated into a deep graph matching network.
- We built new synthetic and real datasets to benchmark scene change detection, which also contain object correspondences and pixel-level change masks between images.

This paper is organized as follows. In Section II, we summarize the related work. Section III and Section IV explain the details of the proposed method and dataset respectively. Section V shows the experimental results and finally, we conclude in Section VI.

Limitations: Our approach can handle change detection where the objects can be clearly detected, but for “stuff” [12] where distinct objects cannot be clearly defined *e.g. pavement, walls, mountains*, object-based detection may not have the advantage we desire. For tasks such as map update for autonomous driving, detecting changes of “semantic objects” such as traffic signals and traffic signs, which indicate traffic rules, is more crucial than detecting changes of “stuff”. Therefore, this study focuses on the change of “things”.

II. RELATED WORK

A. Change Detection

Previous studies have proposed numerous scene change detection methods [13]–[15] for images taken with surveillance cameras [1], [2], satellite and aerial imagery [3]–[6], and vehicular imagery [16], [17]. Previous methods can be divided into two categories, detecting scene change of 2D (image space) or 3D space. In the former category, methods

in [18]–[20] treat a 2D image of a surveillance camera as a background subtraction problem, and model the background image from multiple time periods.

Several methods that detect changes of 3D structures and their texture have also been proposed [7], [21]–[25]. Most of these methods handle the scene depth as unique or probabilistic. They create the scene change model based on the idea, “If there is a change in depth or texture, inconsistencies occur when projecting brightness values or features to images taken at different times”. When an input image pair has a viewpoint difference, pixel-level alignment and high-precision depth maps are necessary.

The recent success of convolutional neural networks (CNNs) enables more accurate and robust change detection [8], [15], [26]–[28], semantic change detection [29], [30] and change captioning [2], [31] in supervised, weakly-supervised [30], [32], semi-supervised [33] and self-supervised [34] manners. The CNNs drastically improve the robustness against changes of camera viewpoint and illumination condition between input images. However, their estimation accuracies are greatly reduced if there is a viewpoint change beyond the range that can be considered with receptive fields of CNNs, because they estimate scene changes by comparing pixels or patches without the concept of objects.

As described in Section I, it is difficult to acquire a precisely aligned image pair that is captured from a vehicle-mounted camera at different time points. And it can reduce the accuracy of change detection methods. The typical approach to solve this problem is to perform registration before change detection. For example, Alcantarilla *et al.* [7] proposed the change detection pipeline that utilizes Simultaneous Localization and Mapping (SLAM) for the image registration. After the alignment, they predict pixel-wise change mask with convolutional neural network (CNN) using deconvolutional layers. However, 3D reconstruction is computationally inefficient and often inaccurate due to changes in the scene or the lack of images. To address this issue, viewpoint-robust change detection methods based on

dense optical flow [35], metric learning [28], and correlation layer [30] have been proposed ever. The motivation of our work is the same as them, but more robust to the large viewpoint difference and requires lower annotation cost.

B. Graph Matching

Graph matching is a problem of finding a one-to-one node mapping between two graphs. It is a fundamental task in computer vision which has many applications, such as key-point matching, template matching, structure from motion, multi-object tracking, and face recognition. The original problem is classified as a quadratic assignment problem (QAP). Since the QAP is known to be NP-hard, we often need to relax the problem in order to solve it directly. Although there are some relaxation and optimization techniques [36], [37] to achieve accurate matching, in this paper we incorporate the deep learning based graph matching method proposed by Zanfir and Sminchisescu [37] to train object-level graph matching efficiently. Different from the above methods, we leverage the epipolar constraint to perform more accurate deep graph matching.

C. Attention-based Segmentation

Zhou *et al.* [38] proposed an attention-based object localization, which requires only image-level annotations for training. They calculate a class activation map from weights and features in the last convolution layer with global average pooling, and it localizes the salient region of an input image. Seo *et al.* propose progressive attention networks (PAN) [39] for attribute prediction, which successively applies attentive processes at multiple layers. Jetly *et al.* [40] extends PAN to general classification networks, and makes it possible to extract the different levels of attended semantic features. Their attention module can readily be incorporated into the object detection network by applying the same attention module not to a whole image but to region of interests (RoIs). In our proposed network, we use attention maps to predict both pixel-wise object segmentation and change maps.

III. METHOD

As shown in Fig. 2, OBJ-CDNet consists of three parts: 1) object detection, 2) object graph matching, and 3) change detection network. From objects detected by the object detection network, the object graph matching network achieves object-level matching through deep graph matching, and the change detection network then estimates changes using features from matched object pairs. In the following, we first briefly introduce graph matching algorithm [37] (Section III-A), then explain the object detection network (Section III-B), the object graph matching network (Section III-C), and the change detection network (Section III-E). In Section III-D, we explain how we can effectively incorporate epipolar constraint into graph matching algorithm.

A. Preliminary

Our object matching network is based on the deep graph matching algorithm proposed in [37]. Below, we briefly introduce the algorithm.

Given two graphs $G_1 = (V_1, E_1)$, $G_2 = (V_2, E_2)$ with nodes V_1 and V_2 ($|V_1| = n$, $|V_2| = m$) and edges E_1 and E_2 ($|E_1| = p$, $|E_2| = q$), the objective of the graph matching algorithm is to find one-to-one mappings of nodes between two graphs based on affinity of node and edge features. Let $\mathbf{x} \in \{0, 1\}^{nm}$ represent the mapping of nodes such that $x_{ij} = 1$ if V_1^i is matched to V_2^j and $x_{ij} = 0$ otherwise. Here, we denote x_{ij} as $(i \times n + j)^{th}$ element of \mathbf{x} . The symmetric affinity matrix, which holds the similarity between nodes and edges, is defined as $\mathbf{M} \in \mathbb{R}^{nm \times nm}$. \mathbf{M} is originally a 4D tensor, which is contracted into a 2D matrix. The diagonal components $\mathbf{M}_{(i_1 i_2, i_1 i_2)}$ depict the correlation of the i_1^{th} node of G_1 and the i_2^{th} node of G_2 . Furthermore, the non-diagonal components $\mathbf{M}_{(i_1 i_2, j_1 j_2)}$ depict the correlation of the edge $(i_1, j_1) \in E_1$ of G_1 and the edge $(i_2, j_2) \in E_2$ of G_2 . The graph matching problem can be formulated as follows:

$$\begin{aligned} \mathbf{x}^* &= \underset{\mathbf{x}}{\operatorname{argmax}} \mathbf{x}^T \mathbf{M} \mathbf{x} \\ \text{s.t. } \mathbf{C} \mathbf{x} &\leq \mathbf{1}_{n+m}, \quad \text{where } \mathbf{C} = \begin{bmatrix} \mathbf{1}_m^T \otimes \mathbf{I}_n \\ \mathbf{1}_n \otimes \mathbf{I}_m^T \end{bmatrix}. \end{aligned} \quad (1)$$

Matrix \mathbf{C} imposes one-to-one constraints. This problem is a quadratic assignment problem and is NP-hard, which means we cannot solve it directly. However, by introducing a unit constraint instead of a one-to-one constraint, we can solve it analytically. The definition is as follows:

$$\mathbf{x}^* = \underset{\mathbf{x}}{\operatorname{argmax}} \mathbf{x}^T \mathbf{M} \mathbf{x} \quad \text{s.t. } \mathbf{x}^T \mathbf{x} = 1. \quad (2)$$

From this, we can achieve the solution \mathbf{x}^* of Eq. (2) as the eigenvector corresponding to the maximum eigen value of \mathbf{M} . By interpreting elements of \mathbf{x}_{ij}^* as the reliability of $i \in V_1$ and $j \in V_2$, we can predict matchings. Since correspondences are determined only by matrix \mathbf{M} , the elements of matrix \mathbf{M} can have a big effect on the accuracy of graph matching. Let the similarity of nodes be $\mathbf{M}_v \in \mathbb{R}^{n \times m}$, and the similarity of edges be $\mathbf{M}_e \in \mathbb{R}^{p \times q}$. With the factorization method proposed in [36], we can obtain \mathbf{M} from \mathbf{M}_e and \mathbf{M}_v .

B. Object Detection Network

In the object detection network, object bounding boxes are detected from each of the input images using Faster R-CNN [41] with ResNet-101 [42]. From each detected bounding box, a feature volume $\mathbf{O} \in \mathbb{R}^{7 \times 7 \times d}$ is obtained through ROI align. The ROI align is applied to the feature map before the last layer of the network. In order to aggregate features inside object regions, object attention maps are further estimated as in [40]:

$$\mathbf{o}_g = \text{GMP}(\text{conv}(\mathbf{O})) \in \mathbb{R}^d \quad (3)$$

$$c_{ij} = \mathbf{u}^T (\mathbf{o}_{ij} + \mathbf{o}_g), \quad \alpha_{ij} = \frac{\exp(c_{ij})}{\sum_{kl} \exp(c_{kl})} \quad (4)$$

where $\text{GMP}(\cdot)$ is Global Max Pooling, $\text{conv}(\cdot)$ represents a convolutional layer, \mathbf{u} are the weight parameters, and \mathbf{o}_{ij} is the feature vector at ij -th spatial location in \mathbf{O} . The attention map α is then used for estimating the change mask in the

downstream change detection network. In addition, α is used for calculating the attended feature vector for the object as follows:

$$\hat{\mathbf{o}}_g = \sum_{ij} \alpha_{ij} \mathbf{o}_{ij} \quad (5)$$

As an alternative to the above attention based method, we also build the detection network based on pre-trained Mask R-CNN [9], and use the segmentation mask from its mask branch as a replacement of the attention map (OBJ-CDSegNet). With the finer pixel-wise segmentation mask from Mask R-CNN, the downstream change detection network can precisely estimate change mask without using pixel-wise change annotations. As we show in Section V, the OBJ-CDSegNet achieves competitive performance to the fully-supervised methods that require pixel-wise change annotations.

C. Object Matching Network

1) *Approach*: The role of object matching network is to find one-to-one matching between detected objects from two input images. In the network, object graphs $G_1(V_1, E_1)$, $G_2(V_2, E_2)$ are first constructed for each of the input images I_1 and I_2 . The detected objects are set as nodes V_1 , V_2 ($|V_1| = n$, $|V_2| = m$), and the edges between nodes are constructed using the Delaunay triangulation ($|E_1| = p$, $|E_2| = q$). The node features $\mathbf{X}_1 \in \mathbb{R}^{n \times (d+2)}$ and $\mathbf{X}_2 \in \mathbb{R}^{m \times (d+2)}$ are obtained for each node by concatenating the attended feature $\hat{\mathbf{o}}_g$ of the node and its coordinate. As proposed in [43], the edge features $\mathbf{H}_1 \in \mathbb{R}^{p \times d}$ and $\mathbf{H}_2 \in \mathbb{R}^{q \times d}$ are taken from RoI pooling of the union bounding boxes of two joined nodes.

From the two graphs G_1 and G_2 , the node affinity matrix $\mathbf{M}_p \in \mathbb{R}^{n \times m}$ is calculated as follows:

$$\mathbf{M}_p = \mathbf{X}_1 \mathbf{X}_2^T \odot \mathbf{W}_e \quad (6)$$

where $\mathbf{W}_e \in \mathbb{R}^{n \times m}$ is a penalization term calculated by epipolar distance between objects. The term effectively incorporates epipolar constraint into the graph matching process; The matched objects should have small epipolar distance. The calculation of the term is explained in Section III-D.

Following [37], the edge affinity matrix $\mathbf{M}_e \in \mathbb{R}^{p \times q}$ is calculated as follows:

$$\mathbf{M}_e = \mathbf{H}_1 \Lambda \mathbf{H}_2^T \quad (7)$$

where $\Lambda \in \mathbb{R}^{d \times d}$ is a block symmetric parameter matrix.

From the affinity matrices, we can obtain matching matrix $\mathbf{S} \in \mathbb{R}^{n \times m}$ using deep graph matching algorithm [37] as:

$$\mathbf{S} = \text{GraphMatch}(\mathbf{M}_p, \mathbf{M}_e) \quad (8)$$

The ij^{th} element of \mathbf{S} represents matching confidence between i^{th} node in V_1 and j^{th} node in V_2 .

It is common to utilize the bi-stochastic constraint – a method to convert the output to a doubly stochastic matrix to improve the accuracy in complete matching problems. However, in our proposed method we allow nodes with no match, thus the constraint is inappropriate, so we do not apply this method.

2) *Training*: During training, a graph matching loss is calculated as a cross entropy loss between the estimated matching matrix \mathbf{S} and the ground truth matching matrix \mathbf{S}^{gt} . In the loss calculation, \mathbf{S} is interpreted as a probability matrix in the following two ways:

$$\mathbf{R}^{1 \rightarrow 2} = \sigma_{row}(\mathbf{S}), \quad \mathbf{R}^{2 \rightarrow 1} = \sigma_{col}(\mathbf{S}) \quad (9)$$

where σ_{row} and σ_{col} represent row- and col-wise softmax operator respectively. $\mathbf{R}^{1 \rightarrow 2}$ and $\mathbf{R}^{2 \rightarrow 1}$ is the matching probability from nodes V_1 to nodes V_2 and from nodes V_2 to nodes V_1 , respectively. The matching loss function can then be as follows:

$$L_{gm}(\mathbf{S}, \mathbf{S}^{gt}) = \sum_{ij} (S_{ij}^{gt} \log R_{ij}^{1 \rightarrow 2} + S_{ij}^{gt} \log R_{ij}^{2 \rightarrow 1}) \quad (10)$$

3) *Inference*: We evaluate the existence of matching at the time of inference, based on the attained matching matrix \mathbf{S} . The one-to-one matching can be established in the following function:

$$\mathbf{S}_{ij} = \begin{cases} 1 & (\text{if } \underset{t}{\text{argmax}} \mathbf{S}_{it} = j \text{ and} \\ & \underset{t}{\text{argmax}} \mathbf{S}_{tj} = i \text{ and } \mathbf{S}_{ij} > \gamma) \\ 0 & (\text{otherwise}) \end{cases} \quad (11)$$

where γ is a hyperparameter that determines the minimum confidence required for the matching. A node $i \in G_1$ and a node $j \in G_2$ are considered as a match if $\mathbf{S}_{ij} = 1$. If no node is matched, that node is labeled as ‘not matched’.

For objects labeled as ‘not matched’, they are immediately classified as ‘changed’, and for objects with matched pair, they are further processed in the succeeding step using change detection network.

D. Epipolar-guided Deep Graph Matching Network

The key idea behind the epipolar-guided deep graph matching network (EGMNet) is to improve the ability to distinguish matching and non-matching objects based on the epipolar constraint between two images in the presence of large viewpoint differences and object detection errors. The constraint can be effectively incorporated into the graph matching network by penalizing the node affinity using epipolar distance between objects (Eq. (6)). The details of EGMNet are described below.

Epipolar distances between the objects are calculated with a fundamental matrix \mathbf{F} . At this point, as it is believed that the larger the rectangular area becomes, the greater the variance of the center coordinate is from the epipolar line, we introduce *normalized epipolar distance* which considers the rectangular area. Here we consider the epipolar distance of $i \in V_1$ and $j \in V_2$. Each coordinate of the node can be written as \mathbf{p}_i and \mathbf{p}_j , hence the epipolar line as $\mathbf{l}_j = \mathbf{F}\mathbf{p}_j$. Therefore, the perpendicular vector \mathbf{v}_{ij} from \mathbf{p}_i to the epipolar line \mathbf{l}_j is described as follows.

$$\mathbf{v}_{ij} = \frac{|\mathbf{p}_i \mathbf{F} \mathbf{p}_j|}{\|\mathbf{l}_j[:2]\|} \mathbf{t} \quad (12)$$

where $\mathbf{x}[:2]$ is a shorthand to represent the first two elements of vector \mathbf{x} and \mathbf{t} is the unit vector in direction \mathbf{v}_{ij} . Let the

height and width of the rectangular area of node j be h_j, w_j . Then, the normalized epipolar distance matrix $\mathbf{D} \in \mathbb{R}^{n \times m}$ is calculated as follows.

$$\mathbf{D}_{ij} = \sqrt{\mathbf{v}_{ij}^T \begin{bmatrix} \frac{1}{w_j^2} & 0 \\ 0 & \frac{1}{h_j^2} \end{bmatrix} \mathbf{v}_{ij}} \quad (13)$$

We finally attain epipolar guided node similarities

$$\mathbf{M}_p = \mathbf{X}_1 \mathbf{X}_2^T \odot \exp\left(-\frac{\mathbf{D}^2}{2\mu_{\mathbf{D}}^2}\right) \quad (14)$$

where $\mu_{\mathbf{D}}$ is the standard deviation of \mathbf{D} . With this operation, we minimize similarities of pairs which have large normalized epipolar distance.

E. Change Detection Network

For each matched object pair obtained from object matching network, the change detection network further classifies if there is a change between objects, and at the same time estimate the change mask. In order to attend to changed region, the change attention maps $\beta_1, \beta_2 \in \mathbb{R}^{7 \times 7}$ are estimated using RoI feature volumes \mathbf{O}_1 and \mathbf{O}_2 of a matched object pair:

$$\mathbf{O}_{\text{diff}} = \mathbf{O}_1 - \mathbf{O}_2 \quad (15)$$

$$\beta_1 = \sigma(\text{conv}_2(\text{conv}_1([\mathbf{O}_1; \mathbf{O}_{\text{diff}}]))) \quad (16)$$

$$\beta_2 = \sigma(\text{conv}_2(\text{conv}_1([\mathbf{O}_2; \mathbf{O}_{\text{diff}}]))) \quad (17)$$

where σ is a softmax operator along the spatial dimensions. From the change attention maps, aggregated feature vector for attended region is obtained:

$$\mathbf{c}_1 = \sum_{ij} \beta_{1,ij} \mathbf{O}_{1,ij} \quad (18)$$

$$\mathbf{c}_2 = \sum_{ij} \beta_{2,ij} \mathbf{O}_{2,ij} \quad (19)$$

During training, we train the feature space using contrastive loss [44] between \mathbf{c}_1 and \mathbf{c}_2 :

$$d = \|\mathbf{c}_1 - \mathbf{c}_2\|_2^2, \quad L_{cd} = td + (1-t)\max(\tau_m - d, 0) \quad (20)$$

where t is a ground truth label ($t = 0$ represent ‘changed’ and $t = 1$ represent ‘not changed’) and τ_m is a margin parameter for the contrastive loss. Once we train the feature space, we can detect change based on the distance between attended features \mathbf{c}_1 and \mathbf{c}_2

Finally, we can also estimate the change masks from the change attention maps and the object attention maps from the object detection network:

$$\mathbf{m}_1 = \alpha_1 \odot \beta_1, \quad \mathbf{m}_2 = \alpha_2 \odot \beta_2 \quad (21)$$

F. Loss Function

We train the three networks shown in Fig. 2 at the same time. We define the loss function as the summation of their loss functions, L_{obj} , L_{gm} , and L_{cd} where L_{obj} is the loss function used in Faster R-CNN [41]. We do not use any weight parameters for three loss terms.

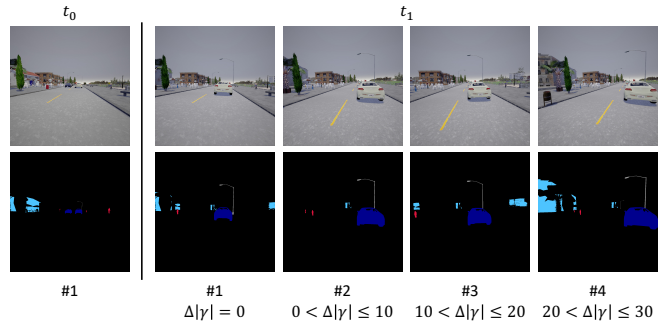


Fig. 3. Examples from the CARLA-OBJCD dataset. There are four pair images per location which have different camera viewpoints.

IV. DATASETS

Although there are several publicly available change detection datasets, such as CD2014 [1], PCD2015 [8] and VL-CMU-CD [7] which contain image pairs and change maps, there is no dataset which contains paired object-level annotations, such as bounding boxes and categories. Therefore, we built synthetic and real datasets for object change detection, called CARLA- and GSV-OBJCD, to evaluate our model and facilitate new researches on both object- and pixel-level scene change detection.

A. CARLA-OBJCD Dataset

This dataset contains 15,000 scene perspective image pairs and their object- and pixel-wise semantic change annotations including object correspondences between images, which are automatically generated under different illumination settings with the CARLA simulator [11]. For evaluation of robustness against camera viewpoint difference, we prepared four variant sets, each of which has 15,000 scenes with different ranges of camera viewpoint difference. The camera pose of the reference image is the same across the four sets, and that of the respective target image varies for the four sets. In set #1, there is no viewpoint difference between reference and target. In sets #2, #3, #4, relative poses of horizontal translation $\Delta x, \Delta y$ [m], roll $\Delta \alpha$ and pitch $\Delta \beta$ [deg] are sampled from the same range $-1 \leq \Delta x, \Delta y \leq 1, -5 \leq \Delta \alpha, \Delta \beta \leq 5$. Only yaw γ [deg] is sampled from different ranges, #2: $0 \leq \Delta|\gamma| \leq 10$, #3: $10 \leq \Delta|\gamma| \leq 20$, and #4: $20 \leq \Delta|\gamma| \leq 30$. We showed the examples of CARLA-OBJCD dataset in Fig. 3.

B. GSV-OBJCD Dataset

This dataset contains 500 pairs of perspective images cropped from Panoramic Semantic Change Detection (PSCD) dataset [30] and manually added annotations of the same type as those in the CARLA-OBJCD dataset (i.e. pixel- and object-wise semantic change labels and matching correspondences of 10388 objects). In contrast to other change detection datasets [7], [8], it is relatively challenging because of the large viewpoint differences and multiple small changes. We believe that the ability to deal with such difficulties is necessary for real applications.

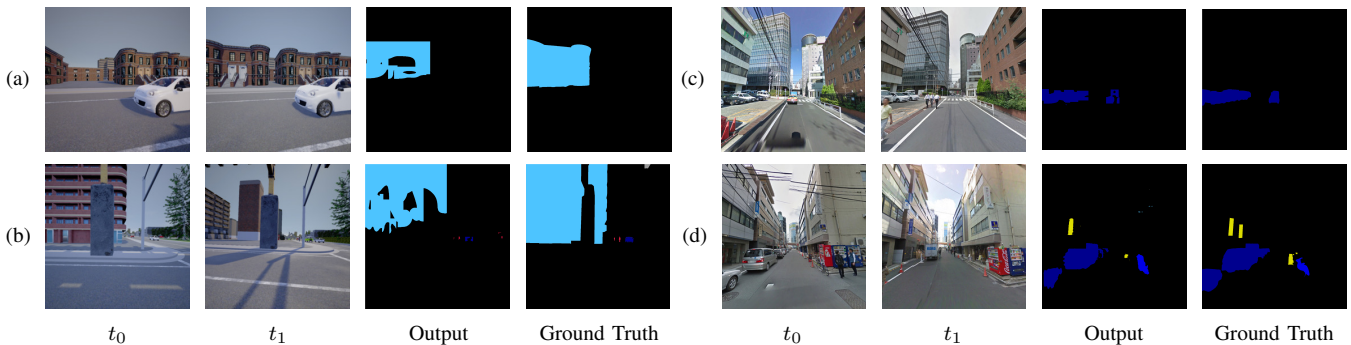


Fig. 4. Qualitative examples of object-based change detection network (OBJ-CDNet). (a), (b) Examples from CARLA-OBJCD dataset. (c), (d) Examples from GSV-OBJCD dataset.

TABLE I

OBJECT MATCHING ACCURACY FOR CARLA- AND GSV-OBJCD DATASETS. DATASET #1 HAS NO VIEWPOINT DIFFERENCE AND #4 HAS THE LARGEST ONES. FC AND DT REPRESENT FULLY CONNECTED AND DELAUNAY TRIANGULATION, RESPECTIVELY.

	CARLA				GSV
	#1	#2	#3	#4	
NN	0.770	0.645	0.644	0.581	0.777
GMN [37]	0.756	0.665	0.666	0.625	0.791
ENN	0.761	0.662	0.662	0.643	0.804
EGMNet (FC)	0.751	0.738	0.736	0.753	0.809
EGMNet (DT)	0.760	0.746	0.747	0.760	0.822

V. EXPERIMENTS

In this section, we describe the two experimental results, both quantitative and qualitative on the synthetic and real image datasets.

A. Implementation Details

During training, we construct object graph from the detected objects that best match ground truth objects based on the IoU between the bounding boxes. For change detection network, we assume correct matching, that is, we calculate the contrastive loss of Eq. (20) for the object pairs in ground truth matching. We set the margin parameter τ_m of the loss as 0.1. As the optimization method, Adam [45] is used with an initial learning rate of 0.001 for the object detection network, 0.0005 for the graph matching network, and 0.005 for the change detection network.

During inference, an object pair is classified as ‘changed’ when the feature distance d in Eq. (20) is larger than 0.05. For the graph matching network, the confidence threshold γ in Eq. (11) is set as 0.5.

We used Faster R-CNN [41] with ResNet-101 [42] as the object detection network, which is pre-trained for 10 epochs on the Cityscapes dataset [10] and then trained for 15 epochs using each target dataset of GSV-OBJCD for fine-tuning. Moreover, we set the hyperparameters as $d = 0.5$, $\mu_D = 2$, $z = 0.1$, and $\tau = 50$.

The pre-training of the OBJ-CDSegNet requires instance mask annotations in addition to bounding box annotations. Since our CARLA- and GSV-OBJCD dataset only have

bounding box annotations, we prepare datasets that have both bounding box and instance mask annotations for pre-training of OBJ-CDSegNet. For the pre-training of the network on CARLA-OBJCD dataset, we newly rendered images with bounding box and instance mask annotations using Carla simulator. For the pre-training of the network on GSV-OBJCD dataset, we used the Cityscapes dataset [10]. We pre-train OBJ-CDSegNet for 15 epochs on the CARLA-OBJCD-rainy dataset and 20 epochs on the Cityscapes dataset. We use Adam as the optimizer and set the learning rate to 1.0×10^{-5} for the object detection network to avoid a decrease in the performance of Mask R-CNN. For other parameters, the same values as OBJ-CDNet are used.

B. Evaluation of Graph Matching

To analyze the effectiveness of deep graph matching network and our proposed epipolar constraint, we conduct detailed experiments on the object matching network with the synthetic dataset.

1) *Dataset*: We use CARLA-OBJCD synthetic dataset, which is described in Section IV-A, with ground truth object bounding boxes and correspondences. We split the image pairs into 10,000/5,000 for training/testing sets. To correctly evaluate generalization error, we use different maps of CARLA simulator for rendering the training and testing images. To analyze the robustness to the viewpoint difference, four different test sets with various viewpoint differences (#1 ~ #4 described in Section IV-A) are used for evaluation.

2) *Metrics*: To test the performance of graph matching, the following metric is used as an accuracy of matching:

$$\text{Accuracy} = \frac{\sum_{p \in P} [p = p^{gt}]}{|P|} \quad (22)$$

where p^{gt} are the ground-truth matched pairs. Let P be the set of matched pairs of graph G_1 and G_2 , and ϕ the pairs with no matched nodes. For instance, the pair with no matched nodes $i \in G_1$ can be described as $p = \{i, \phi\}$, $p^{gt} = \{i, \phi\}$. Then if $p = p^{gt}$, $[p = p^{gt}] = 1$, otherwise 0.

3) *Baselines and proposed method*: We use the following methods as baselines; NN: nearest neighbor matching on deep node features, ENN: a variant of NN that is weighted by the epipolar distance obtained by Eq. (13), and GMN: the

TABLE II

MIOU OF CHANGE DETECTION FOR CARLA-OBJCD DATASET. DATASET #1 HAS NO VIEWPOINT DIFFERENCE AND #4 HAS THE LARGEST ONES.

– Pixel-based method (FS) –	#1	#2	#3	#4
CDNet [35]	0.754	0.602	0.578	0.554
CosimNet-3layer-l2 [28]	0.693	0.610	0.612	0.616
CSCDNet [30]	0.754	0.600	0.605	0.560
– OBJ-CDNet (Att) –	#1	#2	#3	#4
NN	0.552 (0.625)	0.539 (0.608)	0.539 (0.606)	0.535 (0.599)
ENN	0.534 (0.581)	0.518 (0.568)	0.520 (0.569)	0.518 (0.570)
GMN [37]	0.566 (0.637)	0.546 (0.619)	0.554 (0.619)	0.542 (0.607)
EGMNet	0.577 (0.632)	0.531 (0.630)	0.584 (0.630)	0.533 (0.619)
– OBJ-CDSegNet (Seg) –	#1	#2	#3	#4
NN	0.594 (0.661)	0.599 (0.604)	0.597 (0.666)	0.590 (0.656)
ENN	0.595 (0.663)	0.597 (0.658)	0.597 (0.661)	0.598 (0.668)
GMN	0.599 (0.683)	0.598 (0.680)	0.596 (0.678)	0.597 (0.672)
EGMNet	0.596 (0.683)	0.600 (0.684)	0.600 (0.683)	0.605 (0.683)

TABLE III

MIOU OF CHANGE DETECTION FOR GSV-OBJCD DATASET.

– Pixel-based method (FS) –	
CDNet [35]	0.556
CosimNet-3layer-l2 [28]	0.547
CSCDNet [30]	0.583
– OBJ-CDNet (Att) –	
NN	0.471 (0.564)
ENN	0.482 (0.566)
GMN	0.483 (0.567)
EGMNet	0.492 (0.576)
– OBJ-CDSegNet (Seg) –	
NN	0.556 (0.589)
ENN	0.559 (0.587)
GMN	0.558 (0.589)
EGMNet	0.563 (0.593)

graph matching network proposed in [37]. For the proposed methods, we build two variants of EGMNet: EGMNet (FC) and EGMNet (DT) that respectively use fully-connected and Delaunay object graphs.

4) *Results*: Table I shows the object matching accuracies of the baseline methods and ours. For the CARLA-OBJCD synthetic dataset, there is not much difference in their performance when each input image pair has the same viewpoint (set #1). However, the larger the camera pose difference is, the more the matching accuracies of the baseline methods deteriorate. On the other hand, the proposed EGMNet (FC/DT) can keep its accuracy even for large camera pose differences, which confirm the robustness of the method against viewpoint differences. Moreover, EGMNet (FC/DT) outperforms other baseline methods for the GSV-OBJCD real dataset.

Comparing the result of ENN with NN, we can tell that the epipolar constraint plays a significant role in achieving robust matching. Moreover, the use of graph structure also improves matching performance, showing that the relationship between objects is an important cue for the matching.

The graph structure of objects in the scene is not typically apparent. Hence, we compared Delaunay and fully-connected graphs where we defined nodes as the center of the rectangular area. As shown in Table I, EGMNet using the Delaunay graph achieved higher matching accuracy than with a fully-connected one. This result shows that the matching accuracy depends on the geometric relationship of nodes.

C. Evaluation of Pixel-wise Change Detection

The second experiment is the evaluation of pixel-wise change detection accuracy, where we compare our attention- and segmentation-based method with fully-supervised baseline methods.

1) *Dataset*: We use CARLA- and GSV-OBJCD dataset, which is described in Sections IV-A and IV-B respectively, with ground truth object bounding boxes, correspondences, and change masks. The number of samples for training and testing sets are set as 10,000/5,000 for CARLA-OBJCD dataset and 400/100 for GSV-OBJCD dataset. As we do not

have much samples in the GSV-OBJCD dataset, we perform five-fold cross-validation for the dataset.

2) *Baseline*: As the baseline methods, we chose CDNet [35], CSCDNet [30] and CosimNet-3layer-l2 [28], which are state-of-the-art methods for pixel-wise scene change detection. We train them using the ground-truth of the object bounding boxes and instance mask for all the experiments. For the ablation study of object detection, we compare results with and without the ground-truth.

3) *Metrics*: As in previous work [30], [35], we report the mean intersection-over-union (mIoU) of each method for CARLA- and GSV-OBJCD dataset.

4) *Results*: Tables II and III show the pixel-wise change detection accuracy of each method. The scores in the brackets are the values when the ground truth boxes are used instead of the estimated ones to construct the object graphs in our proposed network. Where camera viewpoint differences cause significant performance degradation of the pixel-based baseline methods, OBJ-CDNet and OBJ-CDSegNet can sustain their performance. As [28], [30], [35] predict pixel-level change maps, the more viewpoint changes increase, the more appearance changes increase. However, it is challenging to distinguish these two types of changes based on local features so the error of the change detection increases. Conversely, our method trains graph matching based on bounding boxes, its RoI features, and soft geometric constraints (normalized epipolar distance). The ground-truth of object bounding boxes gives much higher accuracy than object detection, which shows a potential for performance improvement of our method with a more accurate object detection method.

This result also shows that the precise pixel-wise segmentation by transfer learning, compared to an object attention map, improves change detection accuracy considerably. Especially when the viewpoint difference is large, OBJ-CDSegNet outperforms two out of three fully-supervised methods in the CARLA-OBJCD dataset experiments. In GSV-OBJCD dataset experiments, OBJ-CDSegNet attained comparative performance toward fully-supervised methods. As the result of EGMNet with ground-truth of bounding boxes illustrates, as the accuracy of object detection becomes

higher, our network may achieve state-of-the-art performance only by using object-level change annotations.

Figure 4 shows examples of the semantic change detection for OBJCDNet with an attention mechanism. As shown in Fig. 4 (a), (b), and (c), OBJCDNet can accurately detect scene changes even without the change mask annotations. On the other hand, in Fig. 4 (d) the change mask of the small objects is incorrect. This result shows the limitations of our proposed method.

VI. CONCLUSION

This paper proposes an object-based change detection network (OBJ-CDNet) based on an epipolar-guided graph matching network (EGMNet). To the extent of our knowledge, this is the first work to perform object-based scene change detection using an end-to-end deep learning approach, and the first to introduce the epipolar constraint to a graph matching network. Furthermore, we created the first publicly available large-scale dataset to benchmark scene change detection. Our experiments and ablation studies show not only the effectiveness of our approach but also the potential of object-based scene change detection.

ACKNOWLEDGMENT

This work was supported by JSPS KAKENHI Grant Number 20H04217.

REFERENCES

- [1] Y. Wang, P.-M. Jodoin, F. Porikli, J. Konrad, Y. Benezeth, and P. Ishwar, "CDnet 2014: An expanded change detection benchmark dataset," in *CVPR Workshop*, 2014.
- [2] H. Jhamtani and T. Berg-Kirkpatrick, "Learning to Describe Differences Between Pairs of Similar Images," in *EMNLP*, 2018, pp. 4024–4034.
- [3] A. Huertas and R. Nevatia, "Detecting Changes in Aerial Views of Man-Made Structures," in *ICCV*, 1998.
- [4] N. Bourdis, D. Marraud, and H. Sahbi, "Constrained optical flow for aerial image change detection," in *IGARSS*, 2011, pp. 4176–4179.
- [5] D. Crispell, J. Mundy, and G. Taubin, "A Variable-Resolution Probabilistic Three-Dimensional Model for Change Detection," *TGRS*, vol. 50, no. 2, pp. 489–500, 2012.
- [6] T. Pollard and J. L. Mundy, "Change Detection in a 3-d World," in *CVPR*, 2007, pp. 1–6.
- [7] P. F. Alcantarilla, S. Stent, G. Ros, R. Arroyo, and R. Gherardi, "Street-View Change Detection with Deconvolutional Networks," *Autonomous Robots*, vol. 42, no. 7, pp. 1301–1322, 2018.
- [8] K. Sakurada and T. Okatani, "Change Detection from a Street Image Pair using CNN Features and Superpixel Segmentation," in *BMVC*, 2015.
- [9] K. He, G. Gkioxari, P. Dollr, and R. Girshick, "Mask R-CNN," in *ICCV*, 2017.
- [10] M. Cordts, M. Omran, S. Ramos, T. Rehfeld, M. Enzweiler, R. Benenson, U. Franke, S. Roth, and B. Schiele, "The Cityscapes Dataset for Semantic Urban Scene Understanding," in *CVPR*, 2016.
- [11] A. Dosovitskiy, G. Ros, F. Codevilla, A. Lopez, and V. Koltun, "CARLA: An Open Urban Driving Simulator," in *CoRL*, 2017, pp. 1–16.
- [12] A. Kirillov, K. He, R. Girshick, C. Rother, and P. Dollar, "Panoptic Segmentation," in *CVPR*, 2019.
- [13] R. J. Radke, S. Andra, O. Al-Kofahi, and B. Roysam, "Image Change Detection Algorithms: A Systematic Survey," *TIP*, vol. 14, no. 3, 2005.
- [14] D. C. Ibrahim Eden, "Using 3D Line Segments for Robust and Efficient Change Detection from Multiple Noisy Images," in *ECCV*, 2008, pp. 172–185.
- [15] R. C. Daudt, B. Le Saux, and A. Boulch, "Fully convolutional siamese networks for change detection," in *ICIP*, 2018, pp. 4063–4067.
- [16] S. Stent, R. Gherardi, B. Stenger, and R. Cipolla, "Detecting Change for Multi-View, Long-Term Surface Inspection," in *BMVC*, 2015.
- [17] J. Dong, J. G. Burnham, B. Boots, G. Rains, and F. Dellaert, "4D Crop Monitoring: Spatio-Temporal Reconstruction for Agriculture," in *ICRA*, 2017.
- [18] P. Rosin, "Thresholding for change detection," in *ICCV*, 1998, pp. 274–279.
- [19] F. J. López-Rubio and E. López-Rubio, "Features for stochastic approximation based foreground detection," *CVIU*, vol. 133, pp. 30–50, 2015.
- [20] K. Wang, C. Gou, and F.-Y. Wang, "M4CD: A Robust Change Detection Method for Intelligent Visual Surveillance," *IEEE Access*, vol. 6, pp. 15 505–15 520, 2018.
- [21] G. Schindler and F. Dellaert, "Probabilistic temporal inference on reconstructed 3D scenes," in *CVPR*, 2010, pp. 1410–1417.
- [22] A. Taneja, L. Ballan, and M. Pollefeys, "Image based detection of geometric changes in urban environments," in *ICCV*, 2011.
- [23] A. Taneja, L. Ballan, and M. Pollefeys, "City-Scale Change Detection in Cadastral 3D Models Using Images," in *CVPR*, 2013, pp. 113–120.
- [24] K. Sakurada, T. Okatani, and K. Deguchi, "Detecting Changes in 3D Structure of a Scene from Multi-view Images Captured by a Vehicle-Mounted Camera," in *CVPR*, 2013, pp. 137–144.
- [25] K. Matzen and N. Snavely, "Scene Chronology," in *ECCV*, 2014.
- [26] S. Zagoruyko and N. Komodakis, "Learning to compare image patches via convolutional neural networks," in *CVPR*, 2015.
- [27] S. H. Khan, X. He, F. Porikli, and M. Bennamoun, "Forest change detection in incomplete satellite images with deep neural networks," *TGRS*, vol. 55, no. 9, pp. 5407–5423, 2017.
- [28] E. Guo, X. Fu, J. Zhu, M. Deng, Y. Liu, Q. Zhu, and H. Li, "Learning to Measure Change: Fully Convolutional Siamese Metric Networks for Scene Change Detection," *Arxiv*, 2018.
- [29] R. C. Daudt, B. Le Saux, A. Boulch, and Y. Gousseau, "Multitask Learning for Large-scale Semantic Change Detection," *Computer Vision and Image Understanding*, vol. 187, 2019.
- [30] K. Sakurada, M. Shibuya, and W. Wang, "Weakly Supervised Silhouette-based Semantic Scene Change Detection," *ICRA*, 2020.
- [31] D. H. Park, T. Darrell, and A. Rohrbach, "Robust Change Captioning," in *ICCV*, 2019, pp. 4624–4633.
- [32] S. H. Khan, X. He, F. Porikli, M. Bennamoun, F. Sohel, and R. Togneri, "Learning Deep Structured Network for Weakly Supervised Change Detection," in *IJCAI*, 2017, pp. 2008–2015.
- [33] R. Hamaguchi, K. Sakurada, and R. Nakamura, "Rare Event Detection Using Disentangled Representation Learning," in *CVPR*, June 2019.
- [34] Y. Furukawa, K. Suzuki, R. Hamaguchi, M. Onishi, and K. Sakurada, "Self-supervised Simultaneous Alignment and Change Detection," 2020.
- [35] K. Sakurada, W. Wang, N. Kawaguchi, and R. Nakamura, "Dense Optical Flow based Change Detection Network Robust to Difference of Camera Viewpoints," *Arxiv*, 2017.
- [36] F. Zhou and F. D. Torre, "Factorized Graph Matching," *CVPR*, pp. 1–15, 2012.
- [37] A. Zanfir and C. Sminchisescu, "Deep Learning of Graph Matching," in *CVPR*, 2018, pp. 2684–2693.
- [38] B. Zhou, A. Khosla, L. A., A. Oliva, and A. Torralba, "Learning Deep Features for Discriminative Localization," in *CVPR*, 2016, pp. 2921–2929.
- [39] P. H. Seo, Z. Lin, S. Cohen, X. Shen, and B. Han, "Progressive Attention Networks for Visual Attribute Prediction," *BMVC*, pp. 1–19, 2016.
- [40] S. Jetley, N. A. Lord, N. Lee, and P. H. S. Torr, "Learn to Pay Attention," *ICLR*, 2018.
- [41] S. Ren, K. He, R. Girshick, and J. Sun, "Faster R-CNN: Towards real-time object detection with region proposal networks," in *NeurIPS*, 2015, pp. 91–99.
- [42] K. He, X. Zhang, S. Ren, and J. Sun, "Deep Residual Learning for Image Recognition," in *CVPR*, 2016, pp. 770–778.
- [43] T. Yao, Y. Pan, Y. Li, and T. Mei, "Exploring Visual Relationship for Image Captioning," in *ECCV*, 2018.
- [44] R. Hadsell, S. Chopra, and Y. LeCun, "Dimensionality Reduction by Learning an Invariant Mapping," in *CVPR*, 2006, pp. 1735–1742.
- [45] D. Kingma and J. Ba, "Adam: A method for stochastic optimization," in *ICLR*, 2015.